Role of the Distal Hydrogen-Bonding Network in Regulating Oxygen Affinity in the Truncated Hemoglobin III from *Campylobacter jejuni*

Pau Arroyo Mañez,[†] Changyuan Lu,[‡] Leonardo Boechi,[†] Marcelo A. Martí,[†] Mark Shepherd,[§] Jayne Louise Wilson,[§] Robert K. Poole,[§] F. Javier Luque,[||] Syun-Ru Yeh,*[‡] and Darío A. Estrin*[†]

[†]Departamento de Química Inorgánica, Analítica, y Química Fisica, INQUIMAE-CONICET, Facultad de Ciencias Exactas y Naturales, Universidad de Buenos Aires. Ciudad Universitaria, Buenos Aires, Argentina

[‡]Department of Physiology and Biophysics, Albert Einstein College of Medicine, Bronx, New York 10461, United States

[§]Department of Molecular Biology and Biotechnology, The University of Sheffield, Sheffield, United Kingdom

[||]Department de Fisicoquimica and Institut de Biomedicina (IBUB), Facultat de Farmàcia, Universitat de Barcelona, Barcelona, Spain

S *Supporting Information*

ABSTRACT: Oxygen affinity in heme-containing proteins is determined by a number of factors, such as the nature and conformation of the distal residues that stabilize the heme bound-oxygen via hydrogen-bonding interactions. The truncated hemoglobin III from *Campylobacter jejuni* (Ctb) contains three potential hydrogen-bond donors in the distal site: TyrB10, TrpG8, and HisE7. Previous studies suggested that Ctb exhibits an extremely slow oxygen dissociation rate due to an interlaced hydrogen-bonding network involving the three distal residues. Here we have studied the structural and kinetic properties of the $G8_{WF}$ mutant of Ctb and employed state-of-the-art computer simulation methods to investigate the properties of the O_2 adduct of the $G8_{WF}$ mutant, with respect to those of the wild-type protein and the previously studied $E7_{HL}$ and/or $B10_{YF}$ mutants. Our data indicate that the unique oxygen binding properties of Ctb are determined by the interplay of hydrogen-bonding interactions between the heme-bound ligand and the surrounding TyrB10, TrpG8, and HisE7 residues.
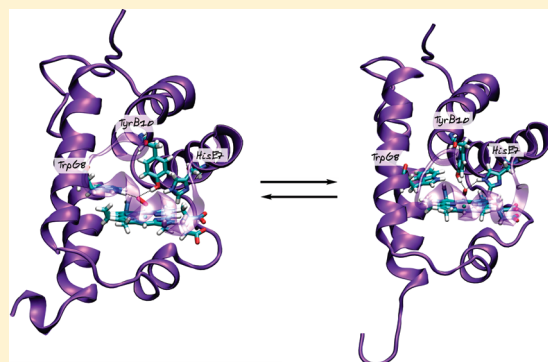
Truncated hemoglobins (trHbs) belong to the hemoglobin superfamily of proteins. They are ~20−40 amino acids shorter than conventional globins. Instead of the 3-over-3 α-helical sandwich motif, trHbs adopt a 2-over-2 α-helical structure.[1,2] Sequence analysis of more than 200 trHbs indicates that they can be divided into three groups: I, II, and III (sometimes referred as N, O, and P, respectively).[2,3] Up to now, most studies on trHbs have been focused on trHb I and II groups of globins,[1,4,5] whereas the group III is much less explored. Nonetheless, recently, the trHb III from the foodborne bacterial pathogen *Campylobacter jejuni*, Ctb, has been structurally and kinetically characterized.[4,6−8]

The globin function is typically characterized by its reactivity toward small ligands, such as O_2, CO, and NO, which bind to the heme distal site.[5,9−11] Among them, O_2 is the most abundant and physiologically relevant ligand. In general, Hbs displaying a moderate oxygen affinity act as O_2 carrier or storage,[1,12] whereas those exhibiting a high oxygen affinity are involved in oxygen chemistry.[4,5,13−16] To perform their designated functions, oxygen affinity of Hbs therefore has to be tightly regulated. The structural basis underlying O_2 affinity of trHbs has been extensively studied.[4−6,11,17−20] These studies show that O_2 affinity is mainly modulated by hydrogen-bonding network

between heme-bound O_2 and amino acid residues located in the distal site of the heme.[11,19] Depending on the distal interactions, oxygen dissociation rate (k_{off}) can vary by more than 5 orders of magnitude.[21] O_2 affinity is also shown to be influenced by the ligand association rate (k_{on}), which is intimately related to the presence of tunnels that facilitate ligand migration from the solvent toward the heme active site.[22,23]

Previous oxygen binding studies of trHb I from *Mycobacterium tuberculosis* (*Mt*-trHbN), an NO dioxygenase,[23,24] showed an unusually high O_2 affinity (K_d = 2.3 nM),[4] allowing oxygen binding even at low O_2 concentrations. The high oxygen affinity of *Mt*-trHbN is achieved by the presence of two polar residues in the distal site, TyrB10 and Gln E11,[13,25] which form hydrogen bonds (HBs) with the heme-bound O_2. Mutation of any of these residues to non-HB-forming residues significantly increases k_{off}.[26] The other trHb from *Mycobacterium tuberculosis*, a trHb II (*Mt*-trHbO), also displays a high O_2 affinity ($K_d \sim$ 11 nM).[4] Although *Mt*-trHbO contains three polar residues in the distal cavity, TyrB10, TyrCD1, and TrpG8, which can donate HBs to

A

the bound O_2, mutation of TyrB10 or TyrCD1 only slightly alter the k_{off}, whereas the mutation of TrpG8 to Phe increases k_{off} by 3 orders of magnitude.[27] Computer simulation studies suggest that the increased k_{off} of the G8 mutant arises from the larger flexibility of the TyrCD1 and LeuE11 side-chain groups.[18] As TrpG8 is conserved throughout groups II and III of trHbs,[28] these data highlight the pivotal role of TrpG8 in the structural and functional properties of these trHbs.

Like *M. tuberculosis*, *C. jejuni* contains two globins, Cgb and Ctb, which belong to the single-domain Hb (sdHb) and trHb III groups, respectively. Neither globin is essential for bacterial growth under laboratory conditions, yet both are up-regulated in response to nitrosative stress.[29,30] Cgb has been suggested to function as a NO dioxygenase, similar to *Mt*-trHbN.[20,31] On the other hand, the physiological function of Ctb is less clear.[4,6] When the Ctb gene is knocked out in *C. jejuni*, the bacterium does not show extra sensitivity to nitrosative stress, but when grown under conditions of high aeration, the bacterium exhibits lowered respiration rates, suggesting a role of Ctb in modulating intracellular O_2 flux.[30,32]

Ctb contains three polar residues in the distal cavity: TyrB10, HisE7, and TrpG8.[8] Previous studies revealed that an intricate HB network involving the three distal polar residues, and the heme-bound ligand in Ctb leads to an extremely high oxygen affinity due to a slow dissociation rate (0.0041 s^{-1}).[6] Using CO as a probe, it was deduced that the electrostatic potential surrounding the ligand increases when TyrB10 and/or HisE7 are mutated to nonpolar substituents,[6] in sharp contrast to the general trend observed in many other Hbs.[4,6] Consistently, either single or double mutation in the TyrB10 and HisE7 residues significantly decreases O_2 dissociation rate.[6] Despite its importance, the mechanism by which the three distal polar residues control oxygen reactivity in Ctb remains unclear.

In order to achieve a comprehensive understanding of the structural role of each distal polar residue in controlling oxygen affinity in Ctb, in this work we examined the structural and kinetic properties of the $G8_{WF}$ mutant of Ctb and compared them with those of the previously studied wild-type enzyme and its $B10_{YF}$ and $E7_{HL}$ mutants. The experimental data are complemented with molecular dynamics (MD) simulations,[9,11,18,33,34] which have been shown to accurately reproduce the structure and dynamics of ligand-bound heme proteins.[10,19,35] In addition, hybrid quantum mechanics—molecular mechanics (QM-MM) were employed to compute the oxygen binding energies of the wild-type and mutant proteins in order to rationalize the experimental data. Our data show that the unusual ligand binding characteristics of Ctb arise from a complex interplay between the structure and dynamics of the three distal polar residues.

■ MATERIALS AND METHODS

Ctb Sample Preparation. The $G8_{WF}$ mutant was prepared using the Stratagene QuikChange site-directed mutagenesis kit. Primers were designed with the codon for the mutated amino acid in the center: forward primer (5′ CACTTAGATCTAC-CTCCTTTTCCTCAAGAGTTTTTTGAAATT**TTT**CTAAAA-CTTTTTGAAGAAAGTTTAAATATAGTTTTAATGAA 3′)-and reverse primer (5′ TTCATTATAAACTATATTTAAA-CTTTCTTCAAAAAGTTTTAG**AAA**AATTTCAAAAAACTC-TTGAGGAAAAGGAGGTAGATCTAAGTG 3′). PCR was carried out on pBAD/His (Invitrogen) carrying the *ctb* gene using primers appropriate for the desired mutation. The PCR

was then incubated with DpnI, an endonuclease specific for methylated DNA. The remaining nonparental mutated DNA was used to transform *Escherichia coli* XL1-Blue supercompetent cells. Constructs were checked by sequencing. The $G8_{WF}$ mutant of Ctb was expressed and purified in the same way as for wt Ctb.[6,7] To form the CO-bound ferrous complexes, $^{12}C^{16}O$ (Tech Air, NY) or $^{13}C^{18}O$ (Icon Isotopes, Summit, NJ) was injected into sodium dithionite-reduced Ctb under anaerobic conditions. The $^{16}O_2$-bound derivative was prepared by passing the CO-bound protein through a G-25 column to allow the exchange of CO with atmospheric $^{16}O_2$ and to remove the excess of dithionite. The $^{18}O_2$-bound sample was prepared by injecting $^{18}O_2$ into an $^{16}O_2$-bound protein solution, followed by spontaneous exchange of heme-bound $^{16}O_2$ with $^{18}O_2$. The concentration of the protein samples used for the Raman measurements was ∼30 μM in 50 mM Tris buffer at pH 7.4 containing 50 μM EDTA.

Resonance Raman Measurements. The resonance Raman (RR) spectra were collected as previously described.[6] Briefly, 413.1 nm excitation from a Kr ion laser (Spectra Physics, Mountain View, CA) was focused to a ∼30 μm spot on the spinning sample cell. The scattered light was collected by a camera lens, dispersed through a polychromator (Spex, Metuchen, NJ), and detected by a liquid nitrogen-cooled CCD camera (Princeton Instruments, Princeton, NJ). A holographic notch filter (Kaiser, Ann Arbor, MI) was used to remove the laser scattering. Typically, the laser power was kept at ∼1 mW and the spectral acquisition time was 60 min. The Raman shift was calibrated by using indene (Sigma) and an acetone/ferrocyanide (Sigma) mixture as the references for the 200−1700 and 1600−2200 cm^{-1} spectral window, respectively.

O_2 Dissociation Kinetic Measurements. The O_2 dissociation reaction was initiated by injecting a small volume (∼50−60 μL) of concentrated O_2-bound protein into a sealed quartz cuvette containing ∼850−900 μL of pH 7.4 buffer (50 mM Tris and 50 μM EDTA) with 1 mM CO. The final concentrations of O_2-bound protein and free oxygen were ∼2−4 and 20 μM, respectively. The reactions were followed at 422 and 405 nm. The dissociation rate constants were calculated based on eq 1:[20]

$$k_{off, O_2} = k_{obs}(1 + k_{on, O_2}[O_2]/k_{on, CO}[CO]) \qquad (1)$$

O_2 Association Kinetic Measurements. The O_2 association reaction was measured with a nanosecond laser flash photolysis system (LKS.60 from Applied Photophysics).[6] In this system, the 532 nm output (∼5 ns, 110 mJ) from a Nd:YAG laser was employed as the photolysis beam. The output from a 150 W xenon arc lamp, at right angles to the photolysis beam, was used as the probe beam. The probe beam passed through a monochromator prior to reaching the quartz cuvette (4 × 10 mm with a 10 mm optical path) containing the sample. The light transmitted through the sample entered a second monochromator, which was synchronized with the first one, and was detected by a photomultiplier tube (1P28 from Hamamatsu Corp.). The signal from the photomultiplier tube was transferred to a digital oscilloscope (Infinium from Agilent Technologies) and then to a personal computer for subsequent analysis. Typically, five or six kinetic traces were averaged to obtain a satisfactory signal-to-noise ratio. The O_2 association reaction was initiated by flashing off CO with the photolysis beam in a freshly prepared mixture of a dithionite-free CO-bound complex (with ∼0.2 mM CO) in the presence of various concentrations of O_2. Under the conditions applied, the rebinding of the CO to the heme iron was much

slower than the O_2 association reactions, which was monitored at 440 nm following the photolysis.

Classical Molecular Dynamics. MD simulations were performed starting from the crystal structure of wild-type (cyano-met form) Ctb (PDB entry 2IG3; monomer A at 2.15 Å resolution)[8] with the CN^- ligand replaced by O_2. The system was immersed in an octahedral box of TIP3P[36] water molecules. Simulations were performed under periodic boundary conditions and Ewald sums[37] for treating long-range electrostatic interactions. The parm99 and TIP3P force fields, which are mean field, nonpolarizable potentials implemented in AMBER, were used to describe the protein and water, respectively. The heme parameters were obtained using the standard Amber protocol from QM calculations on model systems. These parameters have been successfully employed in previous papers of the group.[9−11,19,22−24,37] The nonbonded cutoff used was 9 Å for the minimization and 12 Å for the equilibration and constant-temperature simulations. The temperature and pressure were regulated with the Berendsen thermostat and barostat, respectively, as implemented in AMBER. SHAKE was used to constrain bonds involving hydrogen atoms. The initial system was minimized using a multistep protocol and then heated from 0 to 300 K, and finally a short simulation at constant temperature of 300 K, under constant pressure of 1 bar, was performed to allow the systems to reach proper density. The final structure was used as the starting point for a 50 ns MD simulation at constant temperature (300 K). All mutations were performed *in silico*.

The feasibility of the conformational transition in the $G8_{WF}$ mutant was investigated by computing the free energy profile using umbrella-sampling techniques.[38] To this end, the distance between the hydroxylic hydrogen of TyrB10 and the imidazole N_δ proton of HisE7 was used as distinguished coordinate. A set of windows of 0.1 Å, simulated for 0.4 ns each, was employed to scan the selected coordinate from 5.6 to 1.7 Å. Two independent sets of 12 windows each were employed to estimate the statistical error.

Hybrid Quantum Mechanics−Molecular Mechanics Calculations. The initial structures for the QM-MM calculations[39] were taken from one representative snapshot of each conformation, which were cooled down slowly from 300 to 0 K and subsequently optimized. The iron porphyrinate plus the O_2 ligand and the axial histidine were selected as the QM subsystem, while the rest of the protein and the water molecules were treated classically. All the QM-MM computations were performed at the DFT level with the SIESTA code[40] using the PBE exchange and correlation functional.[41] The frontier between the QM and MM subsystems was treated using the link atom method[42,43] adapted to our SIESTA code. The ferrous pentacoordinated (5c) heme group was treated as a high-spin quintuplet state,[44,45] while the ferrous−O_2 complex was treated as a low-spin singlet state, as they are known to be the ground states of the system. Further technical details about the QM-MM implementation can be found elsewhere.[46]

Binding energies (ΔE) were calculated in selected conformations using eq 2:

$$\Delta E = E_{Heme-O_2} - (E_{O_2} + E_{Heme}) \qquad (2)$$

where E_{Heme-O_2} is the energy of the oxy form of the protein, E_{Heme} is the energy of the deoxy form one, and E_{O_2} is the energy of the isolated oxygen molecule. All the O_2 binding energies for this work were calculated as stated above. Protein fluctuations influence protein−ligand interactions mainly by the dynamics of the H-bonding network, which may present more than one stable conformation.

It is expected that most of protein fluctuation effects are due to these conformations and are of enthalpic nature.

There is a large amount of experimental evidence of the electric field influence on ligand binding in heme proteins. In this context, bound CO has been extensively used as a probe.[47] In order to correlate the simulation results with experimental Raman spectra, we have performed an analysis of the QM-MM optimized structures using Badger's rule,[48] which has been successfully applied to ligand bound heme iron systems:[49,50]

$$r_e = c_{ij}(1/\nu_e^{2/3}) + d_{ij} \qquad (3)$$

where r_e is the equilibrium C−O distance and ν_e refers to $\nu(CO)$. The empirical parameters c_{ij} and d_{ij} were obtained from a fit of the computed optimized bond distances versus the experimental frequencies, 97.919 Å/cm$^{2/3}$ and 0.557 Å, respectively. These empirical values were obtained plotting the RR frequencies vs the C−O bond distance from the QM-MM calculations. The structures for the vibrational calculation were obtained by QM-MM calculations over representative snapshots obtained from MD simulations of the CO complexes.

Furthermore, the electrostatic potential at oxygen atom from the CO ligand was computed for several snapshots taken from the trajectories of each representative conformation (25 snapshots per nanosecond of MD simulation). Electrostatic potential was computed using the following equation:

$$V(r) = \frac{1}{4\pi\varepsilon_0} \sum_i^N \frac{q_i}{|r - r_i|} \qquad (4)$$

where ε_0 is the permittivity in vacuum (8.8542×10^{-12} F/m), q_i is the charge of each atom around the CO (heme atomic charges are not considered),[47] r is the position of the oxygen from the CO ligand, and r_i is the position of the atoms considered to compute the electrostatic potential.

Entropic Contribution Estimation. In this work, we employ a combination of both classical MD simulations to explore the protein conformational space and QM-MM calculations to obtain ligand binding energies with electronic detail. Because of the high computational expense of QM-MM calculations, we performed geometry optimizations in which thermal and entropic effects are not considered. However, on the other hand, in classical MD simulations thermal motions are allowed, and entropic effects are taken into account, since the sampling of different conformations is governed by the actual free energy surface. In order to obtain an estimation of entropic effects on hydrogen-bonding patterns, we have computed entropy, associated with the active site plus the distal aminoacids (TyrB10, HisE7, TrpE15, and TrpG8), by diagonalization of the Cartesian coordinate covariance matrix using the Schlitter method,[51] used in previous works of the group.[52] Because of sampling issues, entropy estimation is dependent on the time window employed, to compute accurate values requires very extended simulations. So, in the case of the entropy contribution to the different conformations, we are conditioned by the time each one remains stable. In spite the entropy is dependent on the sampling time (t), tending to a limit (S_∞) at infinite simulation time.[53] Calculated entropies could be fitted well using the empirical expression

$$S(t) = S_\infty - \frac{\alpha}{t^{2/3}} \qquad (5)$$

■ RESULTS

Equilibrium Structural Properties of the O₂-Adducts. Previous RR work demonstrates that the ν_{Fe-O_2} and ν_{O-O} modes of the oxy derivative of wt Ctb appear at 542 and 1133 cm⁻¹, respectively.[6] The ν_{O-O} mode of heme proteins with His as the proximal ligand is typically silent in RR spectra and was not experimentally observed until recently in several trHbs[6,54,55] its appearance has been linked to a dynamic distal HB network.[1] Likewise, a low ν_{Fe-O_2} (<560 cm⁻¹) has been shown to indicate strong HB interactions between the heme bound ligand and its environment.[6] As shown in Figure 1a, the G8$_{WF}$ mutant exhibits ν_{Fe-O_2} and ν_{O-O} modes at 552 and 1139 cm⁻¹, respectively, pointing to a strong HB interaction between the ligand and the distal residues. As summarized in Table 1, the wild type and all the distal mutants of Ctb show ν_{Fe-O_2} frequencies lower than 560 cm⁻¹, consistent with a distal environment involving multiple H-bonding interactions.

Equilibrium Structural Properties of the CO-Adducts. To further investigate the ligand−protein interactions in Ctb, CO was used as a structural probe for the distal pocket. Figure 1b shows the RR spectra of the $^{12}C^{16}O$ and $^{13}C^{18}O$ derivatives of the G8$_{WF}$ mutant of Ctb. As shown in the $^{12}C^{16}O-^{13}C^{18}O$ difference spectrum, two sets of ν_{Fe-CO}/ν_{C-O} modes were found with values of 499/1963 and 548/1898, which shift to 487/1871 and 534/1812 cm⁻¹, respectively, upon the substitution of $^{12}C^{16}O$ with $^{13}C^{18}O$. It is widely accepted that, when CO is coordinated to the ferrous heme iron, the Fe−CO moiety may be represented by the resonance forms given in eq 6.[56]

$$Fe^{\delta-} - C \equiv O^{\delta+} \text{ (I)} \leftrightarrow Fe = C = O \text{ (II)} \tag{6}$$
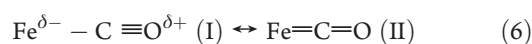
As a general rule, a positive polar environment destabilizes form (I) and facilitates iron π back-bonding interaction, leading to a stronger Fe−CO and weaker C−O bond. On this basis, the ν_{Fe-CO} and ν_{C-O} typically follow a well-known inverse correlation as illustrated in Figure 2a.[56−59] The location of the ν_{Fe-CO}/ν_{C-O} data point on the inverse correlation line is suggestive of the electrostatic potential around the heme-bound ligand.[60] Accordingly, we assigned the two sets of ν_{Fe-CO}/ν_{C-O} modes of the G8$_{WF}$ mutant of Ctb at 499/1963 and 548/1898 cm⁻¹ to an open and a closed conformation, respectively. In the closed conformation (G8$_C$), the heme-bound CO is stabilized by strong HB interactions with its environment, whereas these interactions are absent in the open conformation (G8$_O$).

In the wt protein, only one set of ν_{Fe-CO}/ν_{C-O} modes at 515/1936 cm⁻¹ was observed (located at the middle of the correlation line in Figure 2a), indicating a distal environment with a medium positive electrostatic potential. The B10$_{YF}$/E7$_{HL}$ and B10$_{YF}$ mutations cause the data to shift slightly up along the inverse correlation line, suggesting an increase in the distal electrostatic potential. The E7$_{HL}$ mutation, like the G8$_{WF}$ mutation, leads to the presence of two conformations: one (E7$_{C1}$) looks like G8$_C$, while the other (E7$_{C2}$) resembles the wt protein. The RR data, together with the kinetic data described below, are summarized in Table 1.

Oxygen Dissociation Kinetics. The O₂ dissociation reactions were measured by spontaneous exchange of O₂ in the O₂-bound protein with CO as described in the Materials and Methods section. Figure 2b shows the O₂ dissociation kinetics of the wt and mutant Ctb proteins. All the kinetic traces follow single-exponential functions. As listed in Table 1, the dissociation rate of the G8$_{WF}$ mutant, 0.033 s⁻¹, is significantly faster than those of the wt and other distal mutants, manifesting the importance of the TrpG8 residue in stabilizing heme-bound O₂ in Ctb. However, the rate is still ∼400-fold slower than that of swMb.
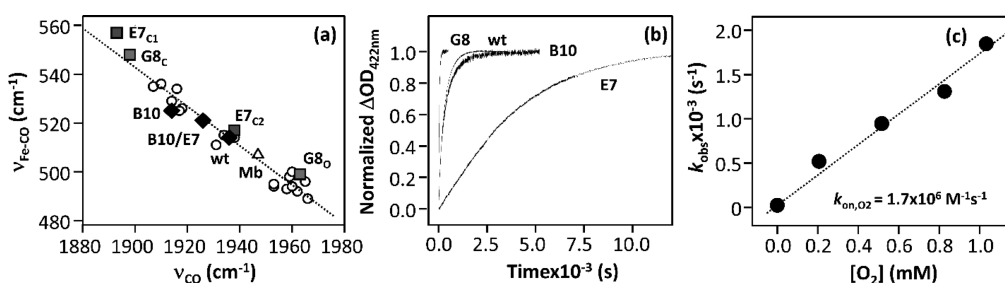
Oxygen Association Kinetics. The O₂ association reaction was measured by flash photolysis of CO from the CO-bound complex in the presence of various concentrations of O₂. The kinetic traces obtained for the G8$_{WF}$ mutant are shown in Figure S1 of the Supporting Information. The bimolecular rate constant, k_{on}, obtained from the concentration-dependent plot (Figure 2c) is 1.7×10^6 M⁻¹ s⁻¹, which is 2-fold faster than that of the wt protein[6] but 8-fold slower than that of swMb (Table 1).
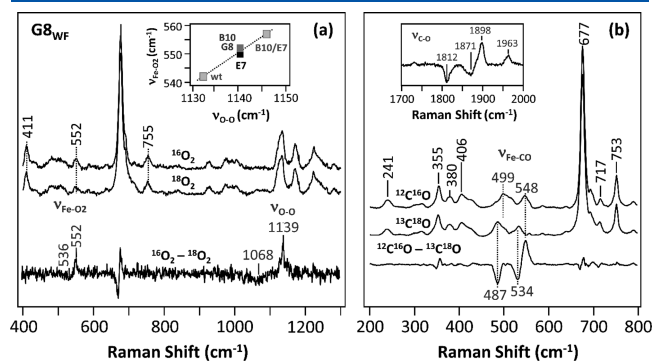

Figure 1. Resonance Raman spectra of the O₂ (a) and CO (b) adducts of the G8$_{WF}$ mutant of Ctb. The data associated with the natural abundant and isotope-labeled ligands and the isotope-difference spectra are as indicated. The inset in (a) shows the correlation between ν_{Fe-O_2} and ν_{O-O}.

Table 1. ν_{Fe-O_2}, ν_{O-O}, ν_{Fe-CO}, and ν_{C-O} Modes Determined by Resonance Raman Spectroscopy, O₂ Dissociation and Association Rate Constants (k_{off} and k_{on}), and O₂ Affinities (K_{O_2}), Calculated from k_{on}/k_{off}, of the Wild Type and Mutants of Ctb, Mt-trHbN, Mt-trHbO, and swMb

species	protein	ν_{Fe-O_2} (cm⁻¹)	ν_{O-O} (cm⁻¹)	ν_{Fe-CO} (cm⁻¹)	ν_{C-O} (cm⁻¹)	k_{on} (μM⁻¹ s⁻¹)	k_{off} (s⁻¹)	K_{O_2} (μM⁻¹)	ref
Ctb (trHbIII)	wt	542	1132	515	1936	0.91	0.0041	222	6
	E7$_{HL}$	550	1139	517, 557	1938, 1891	0.49	0.0003	1885	6
	B10$_{YF}$	552	1139	524	1914	0.12	0.0027	44	6
	B10$_{YF}$/E7$_{HL}$	557	1144	521	1926	42	0.0028	15 000	6
	G8$_{WF}$	552	1139	499, 548	1963, 1898	1.7	0.033	52	this work
Mt-trHbO (trHbII)	wt	559	1140	525	1914	0.13	0.0014	93	4, 26, 54
							0.0058	22	
Mt-trHbN (trHbI)	wt	562	1139	500, 535	1916, 1960	71	0.16	444	4, 13, 63
swMb	wt	569		508	1947	17	15	1.1	1, 67

Figure 2. ν_{Fe-CO}/ν_{C-O} inverse correlation plot (a) and the O_2 dissociation kinetic traces (b) of the wild type and mutants of Ctb, as well as a plot of k_{obs} vs O_2, associated with the O_2 association reaction of the $G8_{WF}$ mutant of Ctb (c). In (a, b) E7, B10, B10/E7, and G8 stand for the $E7_{HL}$, $B10_{YF}$, $B10_{YF}/E7_{HL}$, and $G8_{WF}$ mutants, respectively.
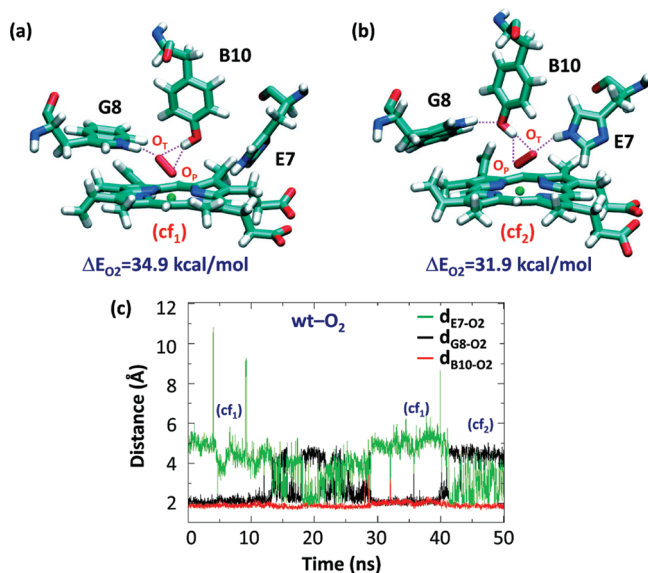
Figure 3. Schematic illustration of the distal site of wt Ctb in two representative conformations (a, b) and the time evolution of d_{B10-O_2}, d_{G8-O_2}, and d_{E7-O_2} during the 50 ns MD simulations of the O_2-adduct (c). The distances associated with potential H bonds, d_{B10-O_2}, d_{G8-O_2}, and d_{E7-O_2}, are defined as the distances between the terminal oxygen of the O_2 ligand and the hydroxylic hydrogen of the TyrB10, the indole Nε proton of the TrpG8, and the imidazolic Nε proton of the HisE7. The O_2-binding energy (ΔE_{O_2}) associated with each conformation in (a, b) resulting from QM-MM calculations is also indicated.

The oxygen affinity (K_{O_2}) of the $G8_{WF}$ mutant, calculated based on the ratio of k_{on} versus k_{off}, is 52 μM^{-1}, which is 4-fold lower than the wt protein but is ~40-fold higher than that of swMb. As listed in Table 1, the distal mutations in Ctb cause the oxygen affinity to vary over 3 orders of magnitude, highlighting the importance of the HB interactions involving TyrB10, HisE7, and TrpG8 in controlling ligand binding in Ctb.

MD Simulations of the Wild-Type Protein. To investigate the molecular details governing the ligand−protein interactions in the O_2-adducts of Ctb, 50 ns MD simulation was performed on the oxygenated wt protein. Visual inspection of the distal site reveals two distinct conformations, cf_1 and cf_2 (Figure 3a,b), which interconvert along the time scale of the MD simulation (see Figure 3c).

In both cf_1 and cf_2, TyrB10 interacts with the bound oxygen, by forming stable HBs with both the terminal (O_T) and proximal oxygen (O_P) atoms. In addition, in cf_1, the Fe−O−O moiety

points toward TrpG8. As a consequence, TrpG8 is strongly hydrogen bonded to the O_T atom (2.13 $\pm$ 0.27 Å), while the HisE7 is 4.65 $\pm$ 0.78 Å away from the O_T atom. In cf_2, the Fe−O−O moiety points to the HisE7 due to its ~180° rotation along the Fe−O_P bond, and a new HB is established between HisE7 and O_T (2.21 $\pm$ 0.33 Å). In this state, TrpG8 forms a HB with TyrB10, keeping the TrpG8 far from the dioxygen ligand. In general, both cf_1 and cf_2 are stable and well-sampled during the time course of the simulation; the heme-bound dioxygen ligand always accepts two HBs from the TyrB10 and one additional HB from either TrpG8 or HisE7 (in cf_1 and cf_2, respectively).

The deoxy derivative of the wt protein was also examined. The TyrB10 forms an HB with the HisE7 for the majority of the simulation time window (see Figure S2a in Supporting Information). This HB breaks occasionally, and the breaking is associated with the movement of TyrB10 toward the TrpG8 and TyrE15, with an averaged d_{B10-G8} significantly longer than $d_{B10-E15}$. In the absence of this HB, HisE7 has no interactions and is able to change the conformation of its side chain in a similar way of the well accepted "E7 gate" in Mb.[61,62] This conformation was observed in the X-ray structure.[8] Once the O_2 binds to the iron, a new HB between TyrB10 and the bound ligand is established, disrupting the TyrB10−HisE7 interaction (see Figure S2 in Supporting Information) and promoting oxygen interaction with TrpG8. During the simulation, several water molecules occasionally enter into the distal pocket and interact with the distal polar residues. This event has been observed in some MD simulations in both the presence and absence of ligand in the distal site. In any case, in the simulations, water molecules used different pathways, and their study is outside the scope of this work.

MD Simulations of the Distal Ctb Mutants. Like wt protein, the MD simulation of the $G8_{WF}$ mutant shows the interconversion between two conformations that exhibit distinct HB interactions (Figure 4). In cf_1, TyrB10 donates a HB to O_T (2.08 $\pm$ 0.29 Å), while HisE7 forms HBs with both oxygen atoms. In cf_2, the side chain of HisE7 rotates ~180° along the $C_\beta-C_\gamma$ bond to accept an HB from TyrB10, preventing both distal residues forming HBs with the heme-bound ligand. In general, the heme-bound dioxygen accepts either 2−3 or 0 HB (Figure 4, a and b, respectively) from the surrounding environment. Extending the MD simulation to 80 ns (see Figure S3 in Supporting Information), the conversion of TyrB10 back to the cf_1 conformation was observed during almost 10 ns. Taken together this fact and the results obtained for the wt Ctb, where TyrB10 seems to be the most important residue stabilizing the bound ligand, this behavior suggests that both conformations contribute significantly
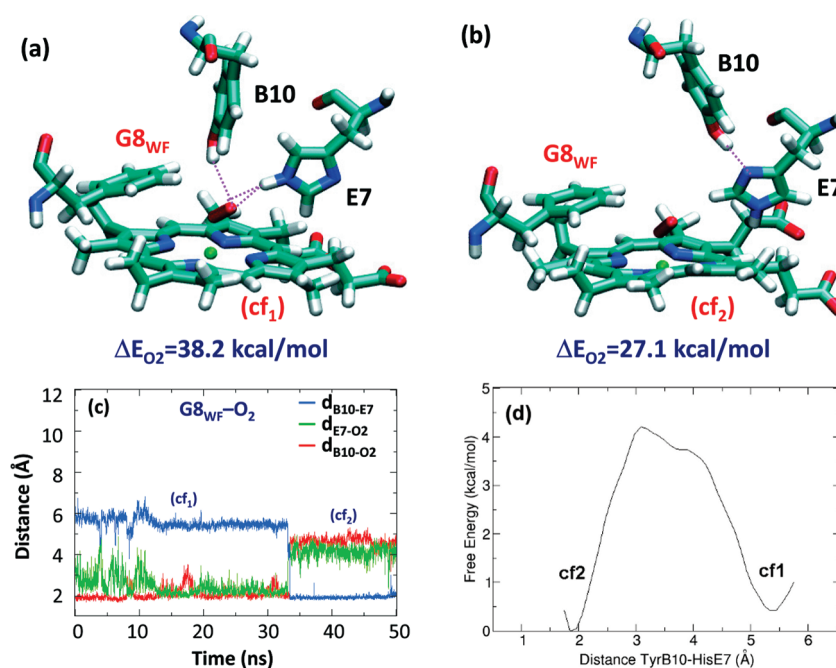
Figure 4. Schematic illustration of the distal site of $G8_{WF}$ mutant of Ctb in two representative conformations (a, b) and the time evolution of d_{B10-E7}, d_{B10-O_2}, and d_{E7-O_2} during the 50 ns MD simulations of the O_2-adduct (c). The distances associated with potential HBs, d_{B10-E7}, d_{E7-O_2}, and d_{B10-O_2}, are defined as the distances between the hydroxylic hydrogen of the TyrB10 and the imidazolic $N\delta$ proton of the HisE7 and between the terminal oxygen of the O_2 ligand and the hydroxylic hydrogen of the TyrB10 and the imidazolic $N\varepsilon$ proton of the HisE7, respectively. The O_2-binding energy (ΔE_{O_2}) associated with each conformation in (a, b) resulting from QM-MM calculations is also indicated. The free energy profile associated with the transition between cf_1 and cf_2 is depicted in panel d. The distance associated with the energetic profile is defined as the distances between the hydroxylic hydrogen of the TyrB10 and the imidazolic N_δ proton of HisE7.

to the network of HB interactions present in the distal cavity of the G8 mutant oxy derivative. Moreover, the MD simulations indicate that the intercorversion between those conformations occurs in a time scale lower than that required for ligand dissociation. To determine the feasibility of the transition between both conformations, an umbrella sampling calculation was performed. The calculated free energy barrier, around 4 kcal/mol, agrees with the observation of interconversion between those conformations along the time scale of the simulation at room temperature (Figure 4d). In addition, to consider entropic effects in the hydrogen-bonding pattern in the $G8_{WF}$ mutant Ctb, we estimated entropy using the Schliter method using a sampling time of 15 ns. The value obtained ($T\Delta S$ 0.51 kcal/mol) indicates, as expected, the minor influence of the entropic effects in this particular conformational exchange.

The MD simulation of the $E7_{HL}$ mutant shows only one stable conformation (Figure 5a), where the O_T of the dioxygen ligand is stabilized by two HBs from TrpG8 (2.11 ± 0.29 Å) and TyrB10 (1.89 ± 0.17 Å), similar to the cf_1 of the wt protein. As indicated by the asterisks in Figure 5a,b, an additional longer HB between the TyrB10 and the O_P of the ligand can be formed transiently, with a mean distance of 2.44 ± 0.24 Å. During the time scale of the simulation, the LeuE7 side chain remains inside the heme pocket as its hydrophobic nature prevents its movement into the solvent. As compared to the wt protein, the data show that HisE7 is important in stabilizing cf_2 by positioning the Fe−O−O moiety in an appropriate orientation for interaction with the TyrB10−TrpG8 pair.

In the $B10_{YF}$ mutant, TrpG8 forms an HB with O_T (2.38 ± 0.99 Å) during most of the simulation time (Figure 5c,d). Occasionally, this HB is broken due to rotation of the Fe−O−O moiety toward

HisE7, with concomitant formation of a new HB between HisE7 and O_T, as indicated by the asterisks. This conformational shift is similar to that observed in the wt protein, although in the absence of TyrB10 cf_1 is strongly favored.

Additional mutation of HisE7 to Leu in the $B10_{YF}$ mutant (leading to the $B10_{YF}/E7_{HL}$ double mutant) does not significantly alter the structural dynamics (Figure 5e,f), indicating that the transient HB interaction between HisE7 and the dioxygen ligand in the $B10_{YF}$ mutant is not critical for ligand escape. This scenario is consistent with the observation that the O_2 dissociation rate constants for the $B10_{YF}$ and $B10_{YF}/E7_{HL}$ mutants are very similar.

QM-MM Calculations of Oxygen Binding Energies. To estimate the protein−oxygen interaction in each representative Ctb structure obtained from the MD simulations, hybrid QM-MM calculations were performed to calculate the ligand binding energies of the O_2-adducts. The results are listed in Table 2. No significant differences were observed for the geometric properties of the Fe−O−O moiety in all the energy-minimized structures of the various derivatives of Ctb. On the other hand, the charge on the heme-bound O_2 (q_{O_2}) estimated using Mulliken populations varies significantly, ranging from −0.263 to −0.403. Nonetheless, the observed negative changes are consistent with the superoxide character of the bound dioxygen as revealed by the RR data (i.e., the ν_{O-O} modes at 1132−44 cm^{-1}). The difference in q_{O_2} indicates that the heme-bound ligand in each protein derivative is differentially polarized by the unique ligand environment with distinct electrostatic potential.

The calculated O_2 binding energies (ΔE_{O_2}) range from 27.1 to 38.2 kcal/mol. As expected, ΔE_{O_2} values correlate with the number of HBs to the heme-bound ligand: the larger the number
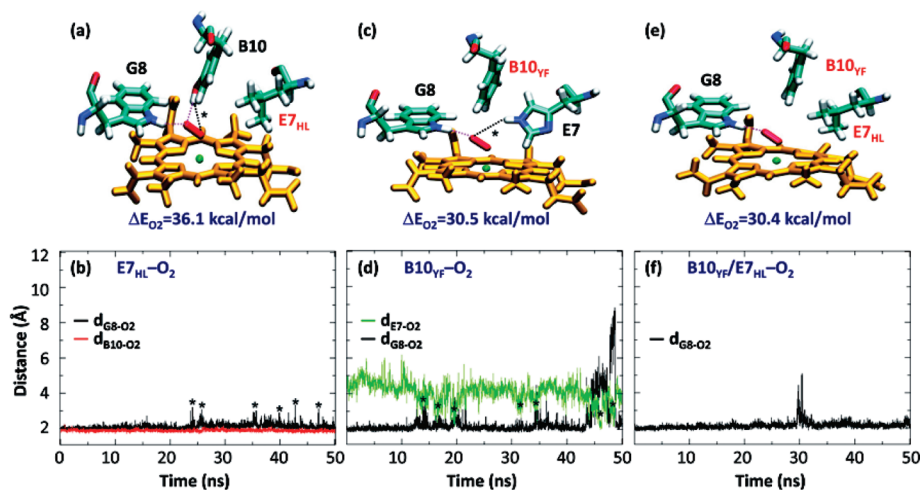
Figure 5. Schematic illustration of the distal site of representative conformations of the $E7_{HL}$, $B10_{YF}$, and $B10_{YF}/E7_{HL}$ mutants of Ctb (panels a, c, and e). Time evolution of d_{B10-O2}, d_{G8-O2}, and/or d_{E7-O2} during the 50 ns MD simulations of the O_2-adduct of the $E7_{HL}$, $B10_{YF}$, and $B10_{YF}/E7_{HL}$ mutants of Ctb (panels b, d, and f, respectively). The parameters d_{B10-O_2}, d_{G8-O_2}, and d_{E7-O_2} are defined as the distances between the terminal oxygen of the O_2 ligand and the hydroxyl proton of the TyrB10, the $N\varepsilon$ proton of the TrpG8, and the $N\varepsilon$ proton of the HisE7. These are depicted with red, black, and green lines, respectively. The O_2-binding energy (ΔE_{O_2}) associated with each mutant in (a, c, and e) resulting from QM-MM calculations is listed as a reference. The transient H-bonds labeled in black dotted lines in (a) and (c), associated with the structures indicated by asterisks in (b) and (d), respectively, are described in the text.

Table 2. Structural and Energetic Parameters Obtained from MD simulations and QM-MM Calculations for the wt and Distal Mutants of Ctb^a

protein	wt		$G8_{WF}$		$E7_{HL}$	$B10_{YF}$	$B10_{YF}/E7_{HL}$
conformation	cf_1	cf_2	cf_1	cf_2			
no. of H-bond	3	3	2−3	0	2	1	1
ΔE_{O_2} (kcal/mol)	34.9	31.9	38.2	27.1	36.1	30.5	30.4
d_{Fe-O} (Å)	1.85	1.78	1.78	1.77	1.77	1.77	1.78
d_{O-O} (Å)	1.31	1.30	1.31	1.29	1.31	1.30	1.30
ϕ_{Fe-O-O}	122.0	124.4	122.9	121.9	122.0	122.0	122.1
q_{O_2} (e)	−0.403	−0.337	−0.388	−0.263	−0.367	−0.297	−0.302
k_{off} (s^{-1})	0.0041		0.0330		0.0003	0.0088	0.0028

^{a} The O_2 dissociation rate constants taken from Table 1 are listed as references.

of HBs, the higher the binding energy. In addition, ΔE_{O_2} also reveals subtle differences that arise from the nature and orientation of the involved HBs. For example, comparison of the cf_1 and cf_2 of the wt proteins (both displaying 3HBs) indicates that the HB donated by TrpG8 is stronger than that donated by HisE7, as suggested by the relatively higher binding energy of cf_1 (34.9 vs 31.9 kcal/mol).

Previous computational studies of heme proteins showed that ΔE_{O_2} is strongly correlated with O_2 dissociation rate.[9,11] Accordingly, it is reasonable to expect that differences in O_2 dissociation in the wt protein and its mutants will be mainly determined by the thermal breakage of protein–oxygen interactions in the heme active site. As listed in Table 2, the ΔE_{O_2} values of all derivatives of Ctb are higher than that reported for Mb (27.0 kcal/mol), except the cf_2 of $G8_{WF}$. The observation is consistent with the lower k_{off} observed in all derivatives of Ctb as compared to Mb. Moreover, the $E7_{HL}$ mutant, which displays the lowest k_{off} value, shows the highest binding energy, when the data of $G8_{WF}$ are excluded. The higher dissociation rate of the $G8_{WF}$ mutant suggests that the protein is in a fast equilibrium between the high (cf_1) and low (cf_2) binding energy conformations and that the

ligand dissociation mainly involves the low binding energy conformation (*vide infra*). The reported 10-fold increase in k_{off} for the $G8_{WF}$ mutant corresponds to a $\Delta\Delta G$ of about 1 kcal/mol. Our results (binding energies of 34.9 and 31.9 kcal/mol for the wt and 38.2 and 27.1 kcal/mol for the $G8_{WF}$ mutant) are qualitatively consistent with the experimental value, since there is one conformation of the mutant with lower binding energy. However, due to limitations in sampling and force fields, it is not possible to obtain reliable populations necessary to obtain quantitative predictions.

To correlate the computed values with experiment, C–O frequencies of the conformations obtained from the MD simulations were estimated as well as the electrostatic potential on the oxygen atom of the bound CO ligand (see Table 3). The computed results, both calculated frequencies using eq 3 and electrostatic potential using eq 4, showed a good correlation with experimental data.

■ DISCUSSION

Oxygen affinity is the key point in determining the heme protein function. To understand how structure and dynamics regulate O_2

Table 3. ν_{Fe-CO} and ν_{C-O} Modes Determined by Resonance Raman Spectroscopy, d_{C-O} Obtrained from the QM-MM Calculation of the Representative Conformations Observed in the MD, ν_{C-O} Calculated Using eq 3, and Electrostatic Potential at the Oxygen Atom of the CO in the Wild Type and Mutant Ctb Proteins (Relative to the Wild Type Value)

Ctb protein	RR ν_{Fe-CO} (cm^{-1})	RR ν_{C-O} (cm^{-1})	d_{C-O} (Å)	calc ν_{C-O} (cm^{-1})	ΔV_O (V)
Wt	515	1936	1.187	1935	0.00
E7$_{HL}$	517, 557	1938, 1891	−, 1.196	−, 1895	−, 4.11
B10$_{YF}$	524	1914	1.189	1926	3.04
B10$_{YF}$/E7$_{HL}$	521	1926	1.186	1940	2.32
G8$_{WF}$	499, 548	1963, 1898	1.183, 1.200	1954, 1877	1.59, 4.47

affinity, experimental or theoretical studies are commonly used. In this work we show how combining experimental and computer simulation approaches allows us to gain insight into the molecular basis of protein reactivity and structure.

Structural Basis for the High Oxygen Affinity of Ctb. Since its discovery, the structural characterization of Ctb has been focused on the relative contribution of distal residues to ligand stabilization. Initial mutagenesis studies revealed that neither mutation of HisE7 nor TyrB10 to non-HB-forming residues increases the k_{off}.[6] The elevated k_{off} for the G8$_{WF}$ mutant (10-fold higher than that for wt) presented herein suggests that TrpG8 provides the major contribution to ligand stabilization. Our RR data show that, in general, the heme-bound O$_2$ in the wt and mutants of Ctb is stabilized by unique HB interactions with its surroundings, as all the ν_{Fe-O_2} frequencies are <560 cm^{-1} and the ν_{O-O} are Raman-active.

The MD simulations demonstrate that, in the wt protein, the main residue responsible for oxygen stabilization is TyrB10. Bound oxygen is further stabilized by an additional HB from either TrpG8 (cf$_1$) or HisE7 (cf$_2$), which depends on the orientation of the Fe−O−O moiety (Figure 3a,b). The QM-MM data show that the HB with TrpG8 is stronger than that with HisE7, and therefore mutation of HisE7 leads to a higher binding energy and a lower k_{off} by constraining Ctb to a cf$_1$-like conformation.

In the O$_2$-adduct of the G8$_{WF}$ mutant, two conformations were observed. In cf$_1$ (Figure 4a), the heme-bound O$_2$ is stabilized by both TyrB10 and HisE7. In cf$_2$ (Figure 4b), a strong HB between TyrB10 and HisE7 is established, preventing either residue from interacting with the ligand, leading to low binding energy. The nature of the two conformers observed in the RR data of the G8$_{WF}$ Ctb CO-adduct (Figure 2a) is consistent with the existence of those conformations: the closed one (cf$_1$), which leads to a strong positive polar electrostatic potential around the heme-bound ligand, and the open conformation (cf$_2$), where the electrostatic potential is less positve. The relatively fast O$_2$ dissociation rate of the G8$_{WF}$ mutant (Table 1) indicates that the dissociation reaction is likely influenced by the presence of the exchange between open and closed conformations, which interconverts in a time scale lower than the dissociation of O$_2$ from the heme.

It is important to note that under equilibrium conditions the O$_2$-adduct of the G8$_{WF}$ mutant exhibits only one ν_{Fe-O_2} mode with a relatively low frequency (552 cm^{-1}, see Table 1), indicating the presence of strong HB(s).[6,55] Hence, the data suggest that the equilibrium favors the G8$_C$ conformer. In contrast, the coexistence of both conformations in the CO-adduct of the G8$_{WF}$ mutant indicates that both G8$_C$ and G8$_O$ are populated. The population shift toward G8$_O$ in the CO-adduct presumably reflects the smaller net partial charge of the heme ligand.

Also noteworthy is the fact that in the wt protein the CO-adduct exhibits only one conformation with medium polar electrostatic potential (Figure 2a), while the O$_2$-adduct displays two conformations on the basis of MD simulations (Figure 3a, b). QM-MM studies of the O$_2$-adduct show that the energy difference between these two conformations is small, as compared to the G8$_{WF}$ mutant (∼3 vs 11 kcal/mol). Moreover, in the wt protein both conformations have the same number of HBs with the ligand, suggesting that the difference in the electrostatic potential surrounding the bound CO in the two conformations of the wt protein is too small to be resolved by the RR studies.

Even though more accurate entropic data were computed, the results obtained for the G8$_{WF}$ mutant confirm that the sampling of different conformations is governed by the actual free energy surface.

In the E7$_{HL}$ mutant, the Fe−O−O moiety is preferentially oriented toward TrpG8. The dioxygen ligand is stabilized by HBs donated by TrpG8 and TyrB10, leading to the highest oxygen binding energy and slowest dissociation rate. The HB with TrpG8, however, can be transiently broken due to the rotation of the Fe−O−O moiety. RR studies of the CO-adduct of the E7$_{HL}$ mutant revealed two conformations: E7$_{C1}$ with a G8$_C$-like high positive polar electrostatic potential and E7$_{C2}$ with a wt-like medium positive polar electrostatic potential (Figure 2a). The E7$_{C1}$ likely corresponds to the major conformation observed in the O$_2$-adduct, whereas the E7$_{C2}$ probably corresponds to the transient conformation, in which the HB donated from TrpG8 to the heme ligand is broken.

In the B10$_{YF}$ mutant, the O$_2$ dissociation rate is 2-fold higher than that of the wt protein. MD simulations show that, when TyrB10 is mutated to Phe, the dioxygen ligand loses the constraint imposed by TyrB10; the Fe−O−O moiety rotates toward TrpG8, establishing a single yet strong HB with it. As a result, the oxygen binding energy decreases slightly, leading to a small increase in the k_{off}. This is in contrast to *Mt*-trHbN, where the replacement of TyrB10 with Phe or Leu in *Mt*-trHbN results in a significant increase in the k_{off}[4] due to the lack of TrpG8.

Hydrogen Bonding and the Regulation of Oxygen Affinity. The coexistence of multiple conformations for the residues in the distal cavity, each characterized by a distinct pattern of HB interaction, creates differences in the local polarity and affects the stabilization of the heme-bound ligand in Ctb. The existence of different HB networks is not a unique propety of Ctb. In fact, the plasticity of HB interactions between the heme ligand, TyrB10, Gln *E7*, Gln *E11*, TyrCD1, and/or TrpG8 residues has also been discussed in the single domain Hb from *C. jejuni* and two trHbs from *M. tuberculosis*.[18] In addition, the interplay between distinct HB interactions between the heme ligand, TyrB10, Gln *E7*, and ThrE11 in the CerHb from *Cerebratulus lacteus* nerve tissue and

the trHb I from *Paramecium caudatum*[10,63−65] and those between the heme ligand, TyrB10, and HisE7 in soybean leghemoglobin[65,66] have all been demonstrated to be important for regulating the oxygen affinities of these Hbs.

Physiological Implications. The requirement for a high oxygen affinity of Ctb in *C. jejuni* physiology is at present not understood. However, the microaerophilic lifestyle of this pathogen and a requirement to control intracellular oxygen concentrations and prevent oxidative stress may have resulted in the evolution of a globin with extraordinarily high affinity for oxygen.

■ CONCLUSION

Our results show that oxygen affinity of Ctb is intricately regulated by the existence of different hydrogen-bonding interactions between the heme-bound ligand and the three key distal residues: TyrB10, TrpG8, and HisE7. The results also show that the behavior of each residue is affected by the other residues, and therefore the binding affinity is the result of a cooperative property. The accurate description of the behavior of distal residues in all the studied mutants has potential implications for understanding and predicting O_2 affinity.

■ ASSOCIATED CONTENT

ⓢ Supporting Information. O_2 association kinetic traces for the $G8_{WF}$ mutant of Ctb; time evolution of the intramolecular distances during 50 ns of MD simulation for the deoxy and O_2-bound derivative of wt Ctb; time evolution of the intramolecular distances during 80 ns of MD simulation for the oxy derivative of the $G8_{WF}$ mutant of Ctb. This material is available free of charge via the Internet at http://pubs.acs.org.

■ AUTHOR INFORMATION

Corresponding Author

*Tel 718-430-4234, Fax 718-430-4230, e-mail syeh@aecom.yu.edu (S.-R.Y.); Tel 54-11-4576-3380, Fax 54-11- 4576-3341, e-mail dario@qi.fcen.uba.ar (D.A.E.).

■ ACKNOWLEDGMENT

■ ABBREVIATIONS

Cgb, single domain hemoglobin from *Campylobacter jejuni*; Ctb, truncated hemoglobin III from *C. jejuni*; Hb, hemoglobin; HB, hydrogen bond; Mb, myoglobin; MD, molecular dynamics; QM-MM, quantum mechanics and molecular mechanics; RR, resonance Raman; sdHb, single domain hemoglobin; swMb, sperm whale myoglobin; trHb, truncated hemoglobin; *Mt*-trHbN, truncated hemoglobin I from *Mycobacterium tuberculosis*; *Mt*-trHbO, truncated hemoglobin II from *M. tuberculosis*.

■ REFERENCES

(1) Egawa, T., and Yeh, S. R. (2005) Structural and functional properties of hemoglobins from unicellular organisms as revealed by resonance Raman spectroscopy. *J. Inorg. Biochem. 99*, 72–96.

(2) Wittenberg, J. B., Bolognesi, M., Wittenberg, B. A., and Guertin, M. (2002) Truncated hemoglobins: A new family of hemoglobins widely distributed in bacteria, unicellular eukaryotes, and plants. *J. Biol. Chem. 277*, 871–874.

(3) Vuletich, D. A., and Lecomte, J. T. J. (2006) A phylogenetic and structural analysis of truncated hemoglobins. *J. Mol. Evol. 62*, 196–210.

(4) Lu, C., Egawa, T., Mukai, M., Poole, R. K., and Yeh, S.-R. (2008) Hemoglobins from *Mycobacterium tuberculosis* and *Campylobacter jejuni*: A comparative study with resonance Raman spectroscopy. *Methods Enzymol. 437*, 255–286.

(5) Milani, M., Pesce, A., Nardini, M., Ouellet, H., Ouellet, Y., Dewilde, S., Bocedi, A., Ascenzi, P., Guertin, M., Moens, L., Friedman, J. M., Wittenberg, J. B., and Bolognesi, M. (2005) Structural bases for heme binding and diatomic ligand recognition in truncated hemoglobins. *J. Inorg. Biochem. 99*, 97–109.

(6) Lu, C., Egawa, T., Wainwright, L. M., Poole, R. K., and Yeh, S.-R. (2007) Structural and functional properties of a truncated hemoglobin from a food-borne pathogen *Campylobacter jejuni*. *J. Biol. Chem. 282*, 13627–13636.

(7) Wainwright, L. M., Wang, Y., Park, S. F., Yeh, S.-R., and Poole, R. K. (2006) Purification and spectroscopic characterization of Ctb, a group III truncated hemoglobin implicated in oxygen metabolism in the food-borne pathogen *Campylobacter jejuni*. *Biochemistry 45*, 6003–6011.

(8) Nardini, M., Pesce, A., Labarre, M., Richard, C., Bolli, A., Ascenzi, P., Guertin, M., and Bolognesi, M. (2006) Structural determinants in the group III truncated hemoglobin from *Campylobacter jejuni*. *J. Biol. Chem. 281*, 37803–37812.

(9) Bikiel, D. E., Boechi, L., Capece, L., Crespo, A., De Biase, P. M., Di Lella, S., González Lebrero, M. C., Martí, M. A., Nadra, A. D., Perissinotti, L. L., Scherlis, D. A., and Estrin, D. A. (2006) Modeling heme proteins using atomistic simulations. *Phys. Chem. Chem. Phys. 8*, 5611–5628.

(10) Marti, M. A., Bikiel, D. E., Crespo, A., Nardini, M., Bolognesi, M., and Estrin, D. A. (2006) Two distinct heme distal site states define Cerebratulus lacteus mini-hemoglobin oxygen affinity. *Proteins: Struc. Funct. Bioinf. 62*, 641–648.

(11) Marti, M. A., Crespo, A., Capece, L., Boechi, L., Bikiel, D. E., Scherlis, D. A., and Estrin, D. A. (2006) Dioxygen affinity in heme proteins investigated by computer simulation. *J. Inorg. Biochem. 100*, 761–770.

(12) Olson, J. S., and Phillips, G. N., Jr. (1996) Kinetic pathways and barriers for ligand binding to myoglobin. *J. Biol. Chem. 271*, 17593–17596.

(13) Couture, M., Yeh, S. R., Wittenberg, B. A., Wittenberg, J. B., Ouellet, Y., Rousseau, D. L., and Guertin, M. A. (1999) Cooperative oxygen-binding hemoglobin from *Mycobacterium tuberculosis*. *Proc. Natl. Acad. Sci. U.S.A. 96*, 11223–11228.

(14) Ouellet, Y., Milani, M., Couture, M., Bolognesi, M., and Guertin, M. (2006) Ligand interactions in the distal heme pocket of *Mycobacterium tuberculosis* truncated hemoglobin N: Roles of TyrB10 and GlnE11 residues. *Biochemistry 45*, 8770–8781.

(15) Frey, A. D., and Kallio, P. T. (2003) Bacterial hemoglobins and flavohemoglobins: versatile proteins and their impact on microbiology and biotechnology. *FEMS Microbiol. Rev. 27*, 525–545.

(16) Gardner, P. R., Gardner, A. M., Brashear, W. T., Suzuki, T., Hvitved, A. N., Setchell, K. D., and Olson, J. S. (2006) Hemoglobins dioxygenate nitric oxide with high fidelity. *J. Inorg. Biochem. 100*, 542–550.

(17) Milani, M., Savard, P. Y., Ouellet, H., Ascenzi, P., Guertin, M., and Bolognesi, M. (2003) A TyrCD1/TrpG8 hydrogen bond network and a TyrB10-TyrCD1 covalent link shape the distal heme distal site of *Mycobacterium tuberculosis* hemoglobin O. *Proc. Natl. Acad. Sci. U.S.A. 100*, 5766–5771.

(18) Guallar, V., Lu, C., Borrelli, K., Egawa, T., and Yeh, S.-R. (2009) Ligand migration in the truncated hemoglobin-II from *Mycobacterium tuberculosis*: The role of G8 tryptophan. *J. Biol. Chem. 284*, 3106–3116.

(19) Capece, L., Marti, M. A., Crespo, A., Doctorovich, F., and Estrin, D. A. (2006) Heme protein oxygen affinity regulation exerted by proximal effects. *J. Am. Chem. Soc. 128*, 12455–12461.

(20) Lu, C., Mukai, M., Lin, Y., Wu, G., Poole, R. K., and Yeh, S.-R. (2007) Structural and functional properties of a single domain hemoglobin from the food-borne pathogen *Campylobactor jejuni*. *J. Biol. Chem. 282*, 25917–25928.

(21) Olson, J. S. (1993) Structural determinants of geminate recombination in myoglobin based on site-directed mutagenesis studies. *J. Inorg. Biochem. 51*, 216.

(22) Bidon-Chanal, A., Marti, M. A., Estrin, D. A., and Luque, F. J. (2007) Dynamical regulation of ligand migration by a gate-opening molecular switch in truncated hemoglobin-N from *Mycobacterium tuberculosis*. *J. Am. Chem. Soc. 129*, 6782–6788.

(23) Marti, M. A., Bidon-Chanal, A., Crespo, A., Yeh, S.-R., Guallar, V., Luque, F. J., and Estrin, D. A. (2008) Mechanism of product release in NO detoxification from *Mycobacterium tuberculosis* truncated hemoglobin N. *J. Am. Chem. Soc. 130*, 1688–1693.

(24) Bidon-Chanal, A., Martí, M. A., Crespo, A., Milani, M., Orozco, M., Bolognesi, M., Luque, F. J., and Estrin, D. A. (2006) Ligand-induced dynamical regulation of NO conversion in *Mycobacterium tuberculosis* truncated hemoglobin-N. *Proteins: Struct., Funct., Bioinf. 64*, 457–464.

(25) Ouellet, Y. H., Daigle, R., Lague, P., Dantsker, D., Milani, M., Bolognesi, M., Friedman, J. M., and Guertin, M. (2008) Ligand binding to truncated hemoglobin N from *Mycobacterium tuberculosis* is strongly modulated by the interplay between the distal heme pocket residues and internal water. *J. Biol. Chem. 283*, 27270–27278.

(26) Ouellet, H., Juszczak, L., Dantsker, D., Samuni, U., Ouellet, Y. H., Savard, P.-Y., Wittenberg, J. B., Wittenberg, B. A., Friedman, J. M., and Guertin, M. (2003) Reactions of *Mycobacterium tuberculosis* truncated hemoglobin O with ligands reveal a novel ligand-inclusive hydrogen bond network. *Biochemistry 42*, 5764–5774.

(27) Ouellet, H., Milani, M., LaBarre, M., Bolognesi, M., Couture, M., and Guertin, M. (2007) The roles of Tyr(CD1) and Trp(G8) in *Mycobacterium tuberculosis* truncated hemoglobin O in ligand binding and on the heme distal site architecture. *Biochemistry 46*, 11440–11450.

(28) Milani, M., Pesce, A., Ouellet, Y., Ascenzi, P., Guertin, M., and Bolognesi, M. (2001) *Mycobacterium tuberculosis* hemoglobin N displays a protein tunnel suited for O_2 diffusion to the heme. *EMBO J. 20*, 3902–3909.

(29) Monk, C. E., Pearson, B. M., Mulholland, F., Smith, H. K., and Poole, R. K. (2008) Oxygen- and NssR-dependent globin expression and enhanced iron acquisition in the response of *Campylobacter* to nitrosative stress. *J. Biol. Chem. 283*, 28413–28425.

(30) Wainwright, L. M., Elvers, K. T., Park, S. F., and Poole, R. K. (2005) A truncated haemoglobin implicated in oxygen metabolism by the microaerophilic food-borne pathogen *Campylobacter jejuni*. *Microbiology 151*, 4079–4091.

(31) Elvers, K. T., Wu, G., Gilberthorpe, N. J., Poole, R. K., and Park, S. F. (2004) Role of an inducible single-domain hemoglobin in mediating resistance to nitric oxide and nitrosative stress in *Campylobacter jejuni* and *Campylobacter coli*. *J. Bacteriol. 186*, 5332–5341.

(32) Elvers, K. T., Turner, S. M., Wainwright, L. M., Marsden, G., Hinds, J., Cole, J. A., Poole, R. K., Penn, C. W., and Park, S. F. (2005) NsrR, a member of the Crp-Fnr superfamily from *Campylobacter jejuni*, regulates a nitrosative stress-responsive regulon that includes both a single domain and truncated haemoglobin. *Mol. Microbiol. 57*, 735–750.

(33) Bossa, C., Anselmi, M., Roccatano, D., Amadei, A., Vallone, B., Brunori, M., and Di Nola, A. (2004) Extended molecular dynamics simulation of the carbon monoxide migration in sperm whale myoglobin. *Biophys. J. 86*, 3855–3862.

(34) Golden, S. D., and Olsen, K. W. (2008) Identification of ligand-binding pathways in truncated hemoglobins using locally enhanced sampling molecular dynamics. *Methods Enzymol. 437*, 19.

(35) Capece, L., Estrin, D. A., and Marti, M. A. (2008) Dynamical characterization of the heme NO oxygen binding (HNOX) domain. Insight into soluble guanylate cyclase allosteric transition. *Biochemistry 47*, 9416–9427.

(36) Jorgensen, W. L., Chandrasekhar, J., Madura, J. D., Impey, R. W., and Klein, M. L. (1983) Comparison of simple potential functions for simulating liquid water. *J. Chem. Phys. 79*, 926–935.

(37) Luty, B. A., Tironi, I. G., and van Gunsteren, W. F. (1995) Lattice-sum methods for calculating electrostatic interactions in molecular simulations. *J. Chem. Phys. 103*, 3014–3021.

(38) Leach, A. R. (2001) *Molecular Modelling*, 2nd ed., Prentice Hall, Englewood Cliffs, NJ.

(39) Warshel, A., and Levitt, M. (1976) Theoretical studies of enzymic reactions: Dielectric, electrostatic and steric stabilization of carbonium ion in the reaction of lysozyme. *J. Mol. Biol. 103*, 227–249.

(40) Soler, J. M., Artacho, E., Gale, J. D., García, A., Junquera, J., Ordejón, P., and Sánchez-Portal, D. (2002) The SIESTA method for ab-initio Order-N materials simulations. *J. Phys.: Condens. Matter 14*, 2745.

(41) Perdew, J. P., Burke, K., and Ernzerhof, M. (1996) Generalized gradient approximation made simple. *Phys. Rev. Lett. 77*, 3865.

(42) Eichinger, M., Tavan, P., Hutter, J., and Parrinello, M. (1999) A hybrid method for solutes in complex solvents: Density functional theory combined with empirical force fields. *J. Chem. Phys. 110*, 10452–10467.

(43) Rovira, C., Schulze, B., Eichinger, M., Evanseck, J. D., and Parrinello, M. (2001) Influence of the heme pocket conformation on the structure and vibrations of the Fe-CO bond in myoglobin: A QM/MM density functional study. *Biophys. J. 81*, 435–445.

(44) Scherlis, D. A., Martí, M. A., Ordejón, P., and Estrin, D. A. (2002) Environment effects on chemical reactivity of heme proteins. *Int. J. Quantum Chem. 90*, 1505–1514.

(45) Rovira, C., Kunc, K., Hutter, J., Ballone, P., and Parrinello, M. (1997) Equilibrium structures and energy of iron-porphyrin complexes. A density functional study. *J. Phys. Chem. A 101*, 8914–8925.

(46) Crespo, A., Scherlis, D. A., Marti, M. A., Ordejon, P., Roitberg, A. E., and Estrin, D. A. (2003) A DFT-based QM-MM approach designed for the treatment of large molecular systems: Application to Chorismate Mutase. *J. Phys. Chem. B 107*, 13728–13736.

(47) Phillips, G. N., Jr., Teodoro, M. L., Li, T., Smith, B., and Olson, J. S. (1999) Bound CO is a molecular probe of electrostatic potential in the distal pocket of myoglobin. *J. Phys. Chem. B 103*, 8817–8829.

(48) Badger, R. M. (1935) The relation between the internuclear distances and force constants of molecules and its application to polyatomic molecules. *J. Chem. Phys. 3*, 710–714.

(49) Green, M. T. (2006) Application of Badger's rule to heme and non-heme iron-oxygen bonds: an examination of ferryl protonation states. *J. Am. Chem. Soc. 128*, 1902–1906.

(50) Daskalakis, D., and Varotsis, C. (2009) Binding and docking interactions of NO, CO and O_2 in heme proteins as probed by density functional theory. *Int. J. Mol. Sci. 10*, 4137–4156.

(51) Schlitter, J. (1993) Estimation of absolute and relative entropies of macromolecules using the covariance matrix. *Chem. Phys. Lett. 215*, 617–621.

(52) Capece, L., Marti, M. A., Bidon-Chanal, A., Nadra, A., Luque, F. J., and Estrin, D. A. (2009) High pressure reveals structural determinants for globin hexacoordination: Neuroglobin and myoglobin cases. *Proteins: Struct., Funct., Bioinf. 75*, 885–894.

(53) Harris, S. A., Gavathiotis, E., Searle, M. S., Orozco, M., and Laughton, C. A. (2001) Cooperativity in drug-DNA recognition: a molecular dynamics study. *J. Am. Chem. Soc. 123*, 12658–12663.

(54) Mukai, M., Savard, P. Y., Ouellet, H., Guertin, M., and Yeh, S.-R. (2002) Unique ligand-protein interactions in a new truncated hemoglobin from *Mycobacterium tuberculosis*. *Biochemistry 41*, 3897–3905.

(55) Das, T. K., Couture, M., Ouellet, Y., Guertin, M., and Rousseau, D. L. (2001) Simultaneous observation of the O—O and Fe—O_2 stretching modes in oxyhemoglobins. *Proc. Natl. Acad. Sci. U.S.A. 98*, 479–484.

(56) Li, T., Quillin, M. L., Phillips, G. N., Jr., and Olson, J. S. (1994) Structural determinants of the stretching frequency of CO bound to myoglobin. *Biochemistry 33*, 1433–1446.

(57) Li, X. Y., and Spiro, T. G. (1988) Is bound carbonyl linear or bent in heme proteins? Evidence from resonance Raman and infrared spectroscopic data. *J. Am. Chem. Soc. 110*, 6024–6033.

(58) Vogel, K. M., Kozlowski, P. M., Zgierski, M. Z., and Spiro, T. G. (2000) Role of the axial ligand in heme---CO backbonding; DFT analysis of vibrational data. *Inorg. Chim. Acta 297*, 11–17.

(59) Yu, N.-T., and Kerr, E. A. (1988) in *Biological Applications of Raman Spectroscopy: Resonance Raman Spectra of Hemes and Metalloproteins* (Spiro, T. G., Ed) Vol. 3, pp 39—95, John Wiley & Sons, Inc., New York.

(60) Phillips, G. N., Jr., Teodoro, M. L., Li, T., Smith, B., Gilson, M. M., and Olson, J. S. (1999) Bound CO is a molecular probe of electrostatic potential in the distal pocket of myoglobin. *J. Phys. Chem. B 103*, 8817–8829.

(61) Johnson, J. B., Lamb, D. C., Frauenfelder, H., Müller, J. D., McMahon, B., Nienhaus, G. U., and Young, R. D. (1996) Ligand binding to heme proteins. VI. Interconversion of taxonomic substates in carbonmonoxymyoglobin. *Biophys. J. 71*, 1563–1573.

(62) Merchant, K. A., Noid, W. G., Thompson, D. E., Akiyama, R., Loring, R. F., and Fayer, M. D. (2003) Structural assignments and dynamics of the A substates of MbCO: Spectrally resolved vibrational echo experiments and molecular dynamics simulations. *J. Phys. Chem. B 107*, 4–7.

(63) Yeh, S.-R., Couture, M., Ouellet, Y., Guertin, M., and Rousseau, D. L. (2000) A cooperative oxygen binding hemoglobin from *Mycobacterium tuberculosis*: Stabilization of heme ligands by a distal tyrosine residue. *J. Biol. Chem. 275*, 1679–1684.

(64) Pesce, A., Nardini, M., Ascenzi, P., Geuens, E., Dewilde, S., Moens, L., Bolognesi, M., Riggs, A. F., Hale, A., Deng, P., Nienhaus, G. U., Olson, J. S., and Nienhaus, K. (2004) Thr-E11 regulates O_2 affinity in *Cerebratulus lacteus* mini-hemoglobin. *J. Biol. Chem. 279*, 33662–33672.

(65) Marti, M. A., Capece, L., Bikiel, D. E., Falcone, B., and Estrin, D. A. (2007) Oxygen affinity controlled by dynamical distal conformations: The soybean leghemoglobin and the *Paramecium caudatum* hemoglobin cases. *Proteins: Struct., Funct., Bioinf. 68*, 480–487.

(66) Kundu, S., and Hargrove, M. S. (2003) Distal heme pocket regulation of ligand binding and stability in soybean leghemoglobin. *Proteins: Struct., Funct., Genet. 50*, 239–248.

(67) Springer, B. A., Sligar, S. G., Olson, J. S., and Phillips, G. N., Jr. (1994) Mechanisms of ligand recognition in myoglobin. *Chem. Rev. 94*, 699–714.